J. Min. Metall. Sect. B-Metall. 55 (3) B (2019) 381 - 395

Journal of Mining and Metallurgy, Section B: Metallurgy

THE EFFECT OF ELECTROSLAG REMELTING ON THE CLEANLINESS OF CrNiMoWMnV ULTRAHIGH-STRENGTH STEELS

M. Ali [*a,c], D. Porter [a], J. Kömi [a], E.-P. Heikkinen [b], M. Eissa [c], H. El Faramawy [c], T. Mattar [c]

[a*] Materials and Mechanical Engineering, Centre for Advanced Steels Research, University of Oulu, Oulu, Finland

[b] Process Metallurgy Research Unit, University of Oulu, Oulu, Finland

[c] Steel Technology Department, Central Metallurgical Research and Development Institute (CMRDI), Helwan, Cairo, Egypt

(Received 11 February 2019; accepted 26 August 2019)

Abstract

The cleanliness of ultrahigh-strength steels (UHSSs) without and with electroslag remelting (ESR) using a slag with the composition of 70% CaF_2, 15% Al_2O_3, and 15% CaO was studied. Three experimental heats of UHSSs with different chemical compositions were designed, melted in an induction furnace, and refined using ESR. Cast ingots were forged at temperatures between 1100 and 950 °C, air cooled, and their non-metallic inclusions (NMIs) were characterized using field emission scanning electron microscopy and laser scanning confocal microscopy. Thermodynamic calculations for the expected NMIs formed in the investigated steels with and without ESR were performed using FactSage 7.2 software while HSC Chemistry version 9.6.1 was used to calculate the standard Gibbs free energies (ΔG°). As a result of ESR the total impurity levels (TIL% = O% + N% + S%) and NMI contents decreased by as much as 46 % and 62 %, respectively. The NMIs were classified into four major classes: oxides, sulphides, nitrides, and complex multiphase inclusions. ESR brings about large changes in the area percentages, number densities, maximum equivalent circle diameters, and the chemical composition of the various NMIs. Most MnS inclusions were removed although some were re-precipitated on oxide or nitride inclusions leading to multiphase inclusions with an oxide or nitride core surrounded by sulphide, e.g. ($MnS.Al_2O_3$) and (MnS. TiN). Also, some sulphides are modified by Ca forming (CaMn)S and $CaS.Al_2O_3$. Some nitrides like TiN and (TiV)N are nucleated and precipitated during the solidification phase. Al_2O_3 inclusions were formed as a result of the addition of Al as a deoxidant to the ESR slag to prevent penetration of oxygen to the molten steel.

Keywords: *Ultrahigh-strength steel; Electroslag remelting; Synthetic slag; Non-metallic inclusions; Cleanliness*

1. Introduction

Some engineering applications require ultrahigh-strength combined with high impact toughness in steel. These applications include pressure vessels; automotive, locomotive and truck components; aircraft undercarriage parts; rocket motor cases, missile bodies and offshore platforms; etc. Alloyed steels such as AF-1410, Aermet-100, Hy-180, and HP9-4-20/30 can be used in these applications, but they are very expensive due to their higher content of alloying elements and their manufacturing process costs.

The present work was undertaken in order to extend the studies of Dilmore et al [1], Yan LU et al [2], and Vartanov [3] to help find different routes, e.g. scrap based, air melting routes, to the production of low-cost ultrahigh-strength steel with high impact toughness. Three experimental heats of low to medium carbon low-alloy steel with different chemical compositions were designed and produced through a low-cost production process consisting of air induction melting followed by refining using conventional ESR.

Especially large and angular inclusions, with lower hot deformability than the steel matrix, are detrimental to such properties as ductility, fatigue resistance, toughness, and corrosion resistance. NMIs can be classified as indigenous and exogenous: indigenous inclusions form in the liquid steel as a

**Corresponding author: mohammed.ali@oulu.fi*

https://doi.org/10.2298/JMMB190211042A

CC BY SA

result of internal sources, e.g. due to deoxidation or reoxidation or the formation of sulphides, while exogenous inclusions are created as a result of external sources such as refractory erosion or slag entrainment [4]. NMIs with a low melting temperature, such that they exist as spherical liquid inclusions during steelmaking, are more easily removed from the liquid steel. Also, they have better deformability [5–9]. Cleanliness of steel can be determined by the size, distribution, shape, and number density of NMIs. Various techniques are available to reduce and control NMIs, such as filtration of the melt, inert gas stirring [10], flux and slag absorption [11], inclusion modification [12], dissolved oxygen control, and the use of a protective atmosphere [13,14].

ESR with its relatively low investment and production costs, combined with high metallurgical quality is considered to be one of the most important secondary refining processes. As a result of the removal of NMIs through ESR, the ductility, impact transition temperature and corrosion resistance are improved [15–17]. Some studies [18,19] show that the grain refinement resulting from the addition of inoculants during the ESR process increase the strength of the steel.

The slag plays various roles in ESR, e.g. acting as a source of heat and protecting the melt. It also has a powerful effect on the yield of alloying elements, desulphurization, and removal of exogenous and harmful NMIs. Mattar [20,21] showed that a 70-15-15 slag system consisting of 70% CaF_2, 15% CaO, and 15% Al_2O_3 not only has a high desulphurizing power but also a remarkable effect on NMI counts, sizes and distributions in the steel matrix. Removal of NMIs during ESR occurs mainly at the tip of the electrode by absorption and dissolution in the slag. Many factors influence the cleanliness of ESR treated steel, e.g. furnace atmosphere, NMI content of the consumable electrode, slag composition and amount, melting rate, power input, and steel grade [22].

There is relatively little information about NMI types, amounts and shapes within the present types of ultrahigh-strength steels. Also, studies on the effect of ESR on steel NMI content often lack information about the chemical changes in the NMIs and the secondary NMIs formed during ESR. This work is aimed at using the modern image acquisition tools laser scanning confocal microscopy (LSCM) and scanning electron microscopy (SEM) combined with X-ray energy dispersive spectroscopy (EDS) to obtain high quality images and detailed descriptions of the counts, sizes, shapes, and chemical compositions of the NMIs in forged bars from the same steel produced without and with ESR. Also, thermodynamic calculations for the expected NMIs are included.

2. Materials and methods

UHSSs with different levels of C, Cr, Ni, Mn, and Si have been designed in order to get different combinations of strength and toughness, the aim being that the steels could be used in a wide range of both commercial and military applications. Three experimental heats with the chemical compositions given in Table 1 were designed and produced in the Steel Technology Department, Central Metallurgical

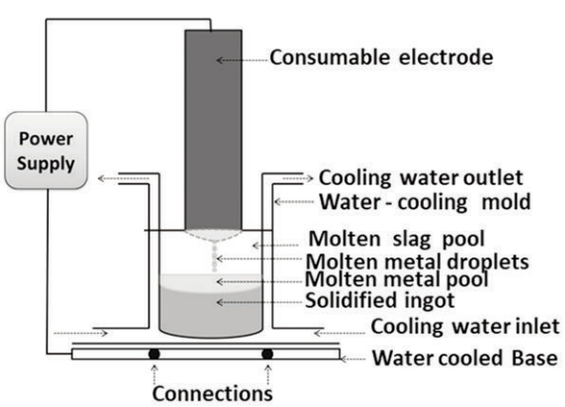

Figure 1. *A schematic diagram of the ESR process*

Table 1. *Chemical compositions of the steels with and without ESR*

Heat No.	Process	Chemical Composition, wt. %																
		C	Cr	Ni	Mo	W	Mn	Si	V	Ti	Nb	Cu	Al	P	S	N	O	TIL*
UHSS I	IF	0.30	2.32	2.34	0.32	1.21	0.70	0.71	0.075	0.001	0.001	0.017	0.009	0.019	0.024	0.013	0.014	0.051
	ESR	0.32	2.18	2.31	0.31	1.14	0.64	0.64	0.072	0.001	0.001	0.020	0.060	0.018	0.013	0.011	0.004	0.028
UHSS II	IF	0.25	2.40	2.49	0.32	1.34	0.57	0.89	0.087	0.002	0.001	0.018	0.009	0.019	0.025	0.020	0.011	0.056
	ESR	0.29	2.37	2.45	0.33	1.23	0.53	0.81	0.085	0.003	0.001	0.020	0.058	0.019	0.014	0.018	0.007	0.039
UHSS III	IF	0.15	1.73	4.44	0.31	1.33	0.41	0.51	0.067	0.002	0.002	0.016	0.009	0.018	0.022	0.022	0.012	0.056
	ESR	0.18	1.65	4.35	0.32	1.24	0.35	0.31	0.062	0.001	0.001	0.020	0.043	0.018	0.017	0.015	0.006	0.038

IF: Ingot Produced from Induction Furnace
ESR: Ingot Produced from Electroslag Remelting Process
* Total impurity levels (TIL, %) = wt.% of S + N + O

CC BY SA

Table 2. *Rules for chemically classifying non-metallic inclusions in the forged IF and ESR ingots*

Classification			Rules (wt., %)
Main class	Name of NMI	Chemical formula	
Sulphides	Manganese sulphide	MnS	Ca<5, O<5, Al<10, Ti<5, N<5, Mn>5, S>5
	Manganese titanium sulphide	(Mn,Ti)S	Ca<5, Al<5, N<5, O<5, Ti>5, Mn>5, S>5
	Calcium manganese sulphide	(Ca,Mn)S	O<5, Al<5, Ca>5, Mn>5, S>5
Oxides	Alumina	Al_2O_3	O>30, Si<5, Mn<5, S<5, Al>20, Ca<5, Ti<5
	Titanium oxide	TiO_2	O>20, Ti>30, Mn<5, Al<10, N<5
	Calcia	CaO	Mn<5, S<5, Al<5, Ti<5, N<5, Ca>5, O>5
	Silica	SiO_2	Si >30, O>5
	Nickel oxide	NiO	Ni>5, O>5, Al<5, Ca<5, Mn<5, Si<5
Nitrides	Titanium vanadium nitride	(TiV)N	V>5, N>5, Ti>20, Mn<5, O<5, S<5
Complex	Aluminosilicate	$Al_2O_3.SiO_2$	Si>5, Al>5, O>5, Ca<5, Cr<5, Mn<5
	Manganese aluminosilicate	$MnO.Al_2O_3.SiO_2$	Al>5, Si>5, Ca<5, S<5, Mn>5, O>5
	Manganese silicate (rhodonite)	$MnO.SiO_2$	Si>10, Al<5, S<5, Mn>5, O>5
	Calcium manganese aluminosilicate	$CaO.MnO.Al_2O_3.SiO_2$	S<5, Al>5, Ca>5, Mn>5, Si>5, O>5
	Manganese sulphide aluminosilicate	$MnS.Al_2O_3.SiO_2$	Mn>5, Al>5, Si>5, Ca<5, S>5, O>5, Ti<5
	Manganese sulphide aluminate	$MnS.Al_2O_3$	Ca<5, Ti<5, N<5, Mn>5, O>5, S>5, Al>5, Ti<5, Si<5
	Manganese oxysulphide	MnOS	Ti<5, Al<5, Ca<5, N<5, Si<5, Mn>5, S>5, O>5
	Manganese sulphide calcium aluminosilicate	$MnS.\ CaO.\ Al_2O_3.SiO_2$	Al>5, Si>5, Ca>5, Mn>5, S>5, O>5
	Manganese sulphide silicate	$MnS.SiO_2$	Si>5, Al<5, Mn>5, S>5, O>5
	Calcium aluminate	$xCaO.yAl_2O_3$	S<5, Mn<5, Ti<5, Ca>5, Ti<5, O>5, S<5, Si<5, Al>10
	Titanium oxide aluminate	$TiO_2.Al_2O_3$	Ca<5, S<5, N<5, Ti>5, O>5, Mn<5, Al>10, Si<5
	Manganese sulphide titanium nitride aluminate	$MnS.TiN.Al_2O_3$	Ca<5, Ti>5, N>10, Mn>5, S>5, O>5, Al>20
	Manganese Oxide aluminate (galaxite)	$MnO.Al_2O_3$	Mn>5, Al>5, O>20, S<5, Ca<5, Si<5
	Manganese sulphide calcium aluminate	$MnS.CaO.Al_2O_3$	Ti<5, N<5, Ca>5, Mn>5, S>5, O>5, Si<5, Al>5
	Manganese sulphide titanium dioxide	$MnS.TiO_2$	N<5, Al<5, Ca<5, Ti>5, Mn>5, S>5, O>5, Al<5, Si<5
	Titanium nitride aluminate	$TiN.Al_2O_3$	Ca<5, S<5, Mn<5, Ti>5, O>5, N>5, Al>5
	Manganese sulphide titanium nitride	MnS.TiN	Al<5, Ca<5, O<5, Ti>5, Mn>5, S>5, V<5, N>5
	Manganese sulphide titanium vanadium nitride	MnS.TiVN	Ti>5, V>5, N>5, Mn>5, S>5, Al<5
	Manganese sulphide titanium oxynitride	MnS.TiON	Ti>5, O>5, N>5, Mn>5, S>5, V<5
	Calcium sulphide aluminate	$CaS.Al_2O_3$	Mn<5, Ti<5, N<5, Ca>5, S>5, O>5, Al>20
	Manganese sulphide titanium dioxide aluminate	$MnS.TiO_2.\ Al_2O_3$	Ca<5, N<5, Ti>5, Mn>5, S>5, O>5, Al>5
	Titanium oxynitride	TiON	Ti>5, Mn<5, Al<5, S<5, Ca<5, N>10, O>5
	Manganese sulphide calcium oxide	MnS.CaO	Al<5, Ti<5, N<5, Ca>5, Mn>5, S>5, O>5, Si<5
	Calcium aluminosilicate	$CaO.Al_2O_3.SiO_2$	Ca>5, Al>5, Si>5, Mn<5, O>5
	Calcium manganese aluminate	$CaO.MnO.\ Al_2O_3$	Ca>5, Mn>5, Al>5, O>5, Si<5, S<5
	Calcium oxysulphide	CaOS	Al<5, Mn<5, Ti<5, N<5, Cr<5, Ca>5, S>5, O>5

CC BY SA

Research and Development Institute (CMRDI) in Egypt by melting recycled steel, ferroalloys and nickel in an air induction furnace lined with spinel. After the chemical composition and the temperature of the molten steel were adjusted, the molten metal was tapped at 1560-1580 °C into a steel mould, 250 mm long and 70 mm in diameter. The produced steel ingots were reheated to 1100 °C and held for 1 hour before forging into bars with a cross section of about 28 mm x 30 mm. Forging started at about 1100 °C and finished at 950 °C followed by air cooling at about 0.3 °C/s. Half of the produced bars were studied in the forged form and the other half was used as consumable electrodes for electroslag remelting under a synthetic fused slag containing about 70% CaF_2, 15% Al_2O_3 and 15% CaO. A small amount of Al metal was added to the slag as a deoxidant at the beginning of the ESR process. The ESR ingot was subsequently forged and cooled using the forging parameters mentioned above. Our previous publication [23] gives details about the production methods of the investigated UHSSs, the chemical compositions of the charging materials, and the composition of the slag used in the remelting process.

The ESR machine consists of a power supply with control of the current and voltage, Fig. 1. The ESR process parameters were: 1200-1500 A, 30-40 V, and 4.63 g/s for current, voltage, and melting rate respectively.

Qualitative and quantitative analysis of NMIs in the forged steels without and with ESR were investigated using two techniques, Laser Scanning Confocal Microscopy (LSCM) together with VK analyzer software and a Zeiss ULTRA Plus field emission scanning electron microscope (FESEM) with an automated particle explorer, INCA software, and Aztec software attached to an energy dispersive X-ray spectrometer (EDS).

LSCM-VK analysis was used to provide statistical analysis of NMIs such as counts, sizes and shapes. The main advantages of this technique are that it provides high-resolution images combined with the possibility of investigating large areas in reasonable times.

Automated FESEM-INCA was used to provide statistical analyses of the observed NMIs including counts, sizes, and shapes in addition to the chemical analysis of all NMIs. The advantages of this technique are that it allows the automatic collection and processing of chemical and stereological data on NMIs. However, compared to LSCM, it is best suited for investigation of small areas. The analysis settings were accelerating voltage 15 kV, aperture size 60 µm, working distance 8.5 mm, magnification 1000, minimum particle size 0.5 µm, and resolution 1024 x 1024 pixels. All detected inclusions were classified according to their elemental composition according to the rules given in Table 2. 12 x 10 x 6 mm samples from the three heats of steel were mounted in a conductive phenolic hot mounting resin with a carbon filler to assist with edge retention and FESEM examination. The samples were ground, polished and ultrasonically cleaned in ethanol to remove any dust or particle contamination on the surface of the sample. In order to easily deal with the variation in the NMI shapes, the inclusion size was characterized by calculating the equivalent circle diameter (ECD) according to the following relation [24]:

$$ECD = \sqrt{4.Area / \pi}$$

Two thermodynamic software packages were used in the current study. FactSage 7.2 [25] together with the databases FSstel, FToxid, and FactPS have been used to calculate the predicted inclusion compositions based on the measured chemical compositions of the investigated steels without and with ESR. HSC Chemistry version 9.6.1 [26] was used to calculate standard Gibbs free energies (ΔG°).

3. Results and Discussion

3.1 Size and frequency of NMIs

A general impression of the degree of cleanliness of the steels processed without and with ESR can be seen in the SEM micrographs in Fig. 2. For the quantitative evaluations of NMIs using LSCM, thirty images were taken per sample covering a total area of 44 mm^2. In the case of quantitative SEM studies, 122 fields covering a total area of 7.3 mm^2 were examined. For both LSCM and FESEM examinations, Fig. 3 and Fig. 4, respectively, show the number per mm^2 and area percentages of NMIs in the steels without and with ESR.

Based on the results from LSCM, ESR reduced the total number of NMIs in UHSSs I, II, III by 43 %, 6 %, and 57 % respectively. In all cases, NMIs with an ECD smaller than 6 µm, which have little effect on steel properties and can be ignored according to the standard DIN 50 602 [27], represent about 94% of the total inclusion counts as compared with 90% without ESR. As is apparent from Fig. 3, for all steels, the number of NMIs per mm^2 in all size ranges decreased as a result of ESR except the number of NMIs per mm^2 in size range 0-3µm in UHSS II. The latter case is due to the dissociation and erosion of larger NMIs and the re-generation of new smaller ones together with some changes in the impurity levels and alloy elements that make up the inclusions, as discussed further below. Fig. 4 shows that the area percentage of NMIs in all size ranges decreased as a result of ESR in all the investigated steels except in the size range 0-3 µm in UHSSs I and II.

Based on the FESEM results, the total number of NMIs decreased in UHSSs I, II, and III by 55 %, 19

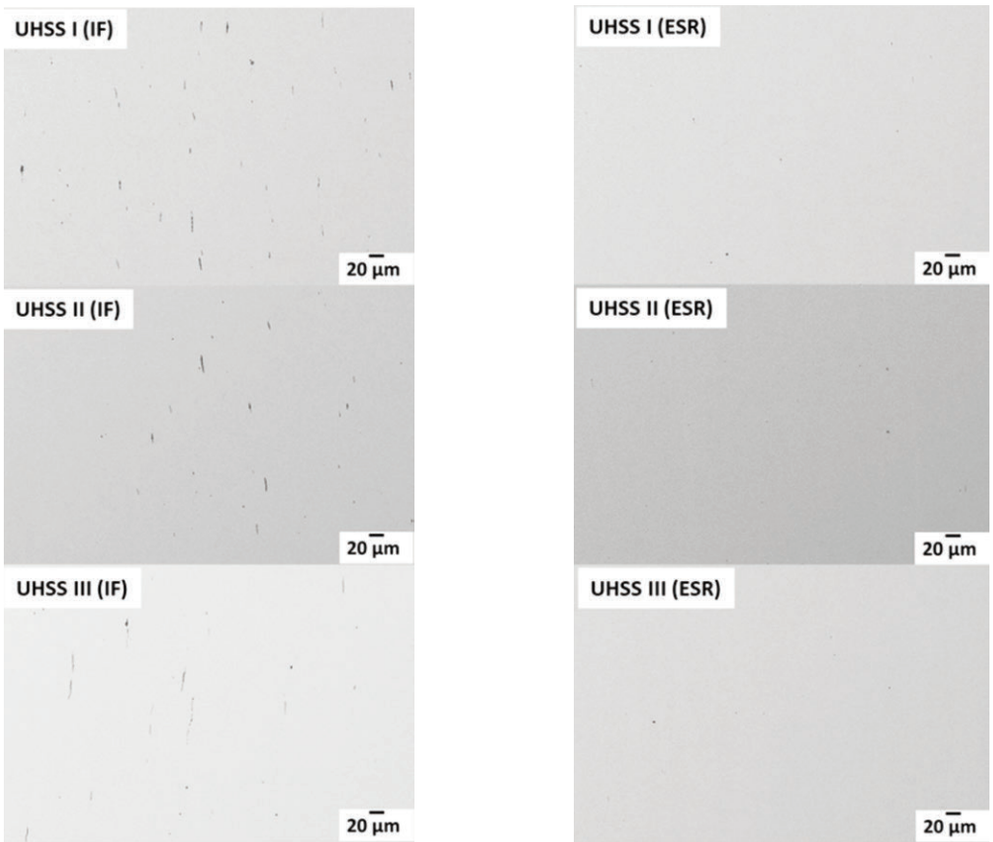

Figure 2. *SEM micrograph of NMIs in UHSS I, II and III without and with ESR*

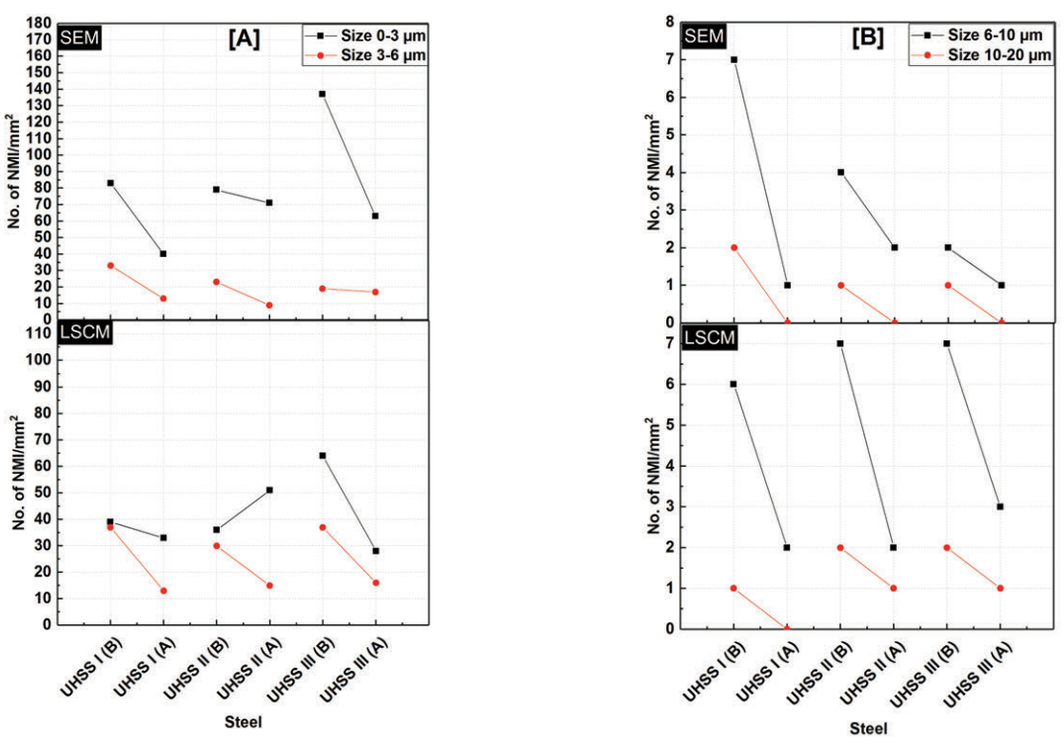

Figure 3. *Number of NMIs per mm² in UHSS I, II and III without and with ESR. Results from SEM and LSCM investigations; [A]: size ranges 0-3µm and 3-6µm; [B]: size ranges 6-10 µm and 10-20 µm*

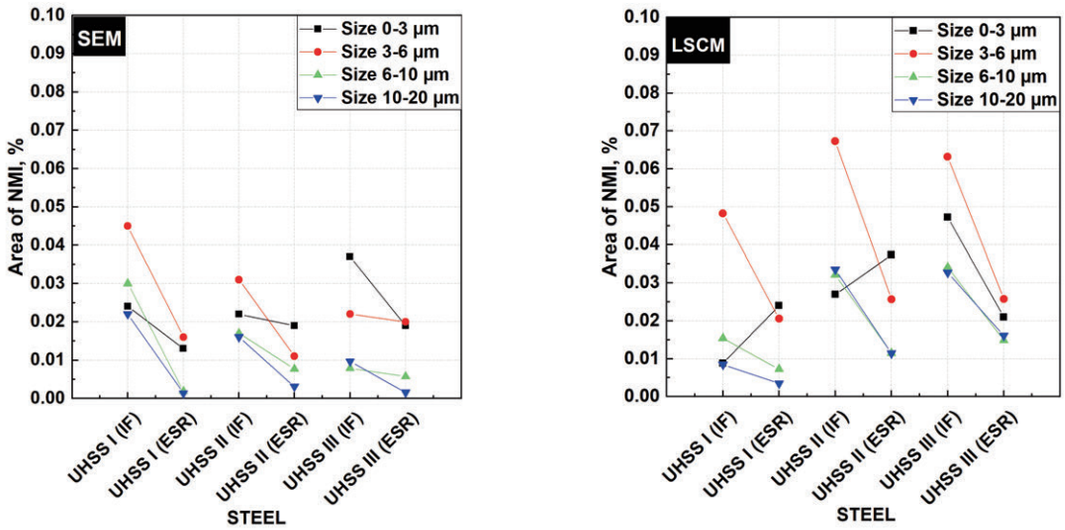

Figure 4. *SEM and LSCM data on area percentages of NMIs without and with ESR*

%, and 62 % respectively. In all cases, NMIs smaller than 6 µm represent about 98 % of the total inclusion counts after ESR as compared with 96 % without ESR. As is apparent from Fig. 3, for all steels, the number of NMIs per mm^2 in all size ranges decreased as a result of ESR. Fig. 4 shows that the area percentage of NMIs in all size ranges also decreased as a result of ESR in all the steels.

Comparing the results obtained by LSCM and FESEM, there are slight differences between the two techniques, which may result from the differences in the total areas investigated (44 vs. 7 mm^2): it was much easier to study large areas with LSCM but, due to its better resolution, the FESEM was better at revealing small inclusions.

There are slight differences in the degree of refining of the investigated steels as measured by the total impurity level (TIL% = S % + N % + O %), NMI area percentages and number densities as can be seen in Fig. 5. Based on the number density and area fraction of NMIs, it can be concluded that UHSSs I and III have the best degree of refining followed by UHSS II. On the other hand, from Fig. 5 it is clear that removing a small number of NMIs by ESR resulted in a big decrease in the area fraction, which indicates that the removed NMIs were large ones.

3.2 Chemical composition of NMIs

The NMIs in all the investigated steels can be divided into four major classes: oxides, sulphides, nitrides, and complex multiphase inclusions. Fig. 6 and Fig. 7 summarize their area percentages, number densities, and maximum ECDs. The large differences in the distribution of the NMIs among the four classes brought about by ESR are discussed in this section.

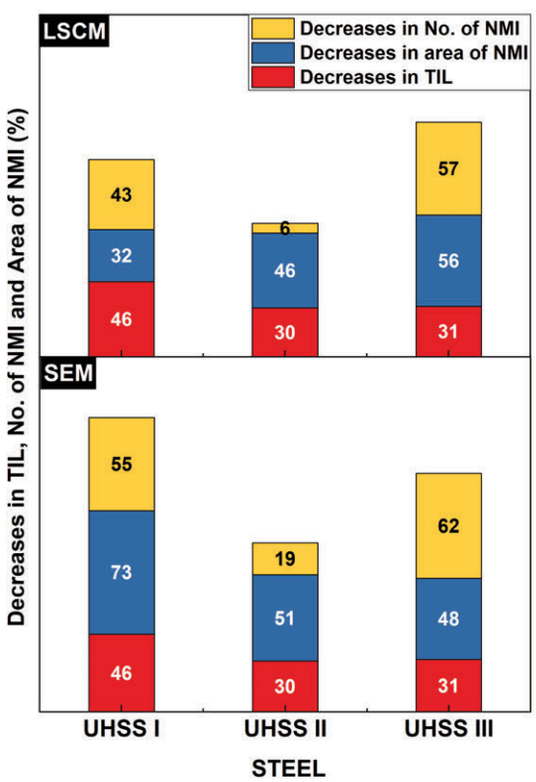

Figure 5. *Percentage reductions in total impurity level, No. of NMIs and area percentage of NMIs as a result of ESR*

The differences are a result of the reactions between the slag and the investigated steels with their different compositions and impurity levels.

As a result of ESR and, as illustrated by Fig. 6 and Fig. 7, the area percentage, numbers, and maximum sizes of all complex inclusions in all the

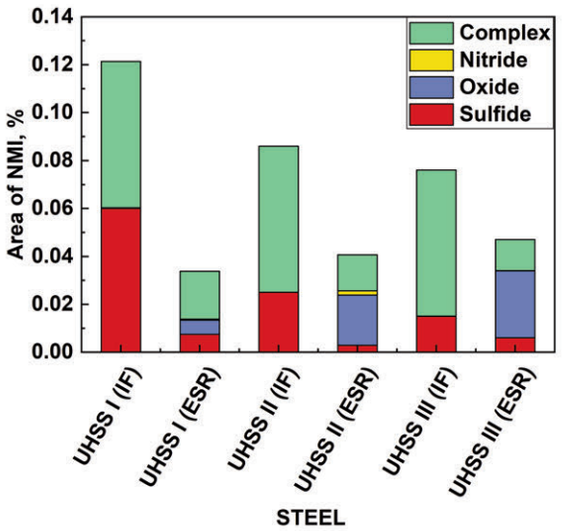

Figure 6. *Area fractions of each class of NMIs without and with ESR*

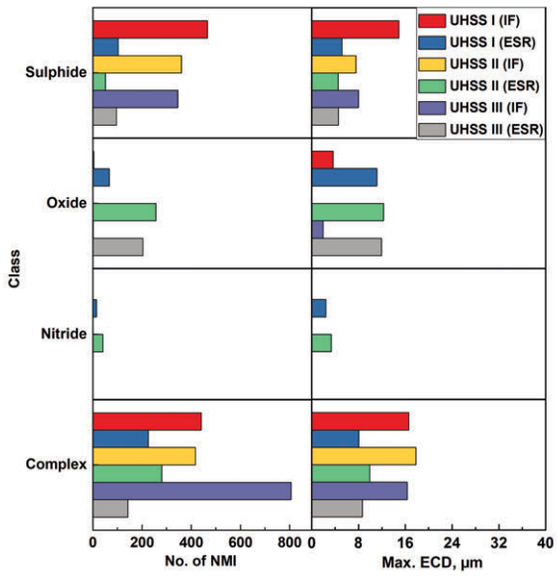

Figure 7. *Number of NMIs and maximum ECD of each class of NMI without and with ESR*

steels are decreased by dissolution of all NMIs and re-generation of new smaller ones. Also, there is a large decrease in the area percentage, numbers, and maximum sizes of all sulphides in all steels. Some nitrides with a small area percentage, number and max ECD are precipitated during ESR in UHSSs I and II. The high temperature of the slag increases the possibility for the dissolution of NMIs [27]. Therefore, both the area fraction and number density of oxides are increased by ESR due to the dissociation and dissolution of complex inclusions and the precipitation of small oxides due to the addition of the Al deoxidant.

The behaviour of NMIs in electroslag refining is related to the different interfaces found in the process, i.e. the slag-air, slag-electrode, slag-droplet and slag-metal pool interfaces as illustrated in Fig. 8a. The slag-electrode interface is the most important position in the ESR process as most of the NMIs are removed there [28]. Details concerning the chemical compositions of the NMIs and their distributions, area fractions, relative numbers and maximum sizes without and with ESR are given in Fig. 9, Fig. 12, and Fig. 14.

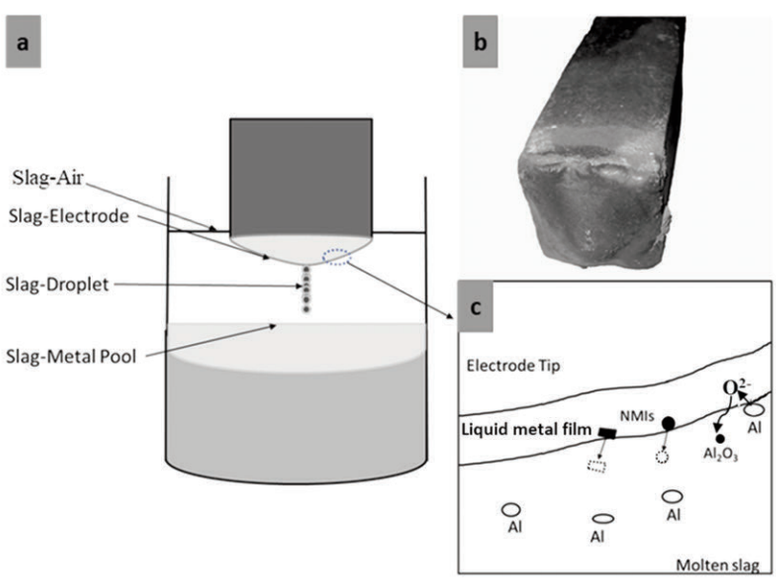

Figure 8. *a) Schematic diagram showing the interfaces in the ESR process. b) Actual electrode tip and liquid metal film formed during ESR process for one of the investigated steels. c) Dissolution of NMIs (rectangles and circles) and Al deoxidation at the liquid metal film formed on the tip of the electrode*

CC BY SA

In UHSS I (Fig. 9), without ESR the NMIs are sulphides, such as MnS and (Mn,Ti)S; pure oxides, such as alumina and complex NMIs such as ($Al_2O_3.SiO_2$), ($MnO.Al_2O_3.SiO_2$), ($MnO.SiO_2$), ($CaO.MnO.Al_2O_3.SiO_2$), ($MnS.Al_2O_3.SiO_2$), ($MnS.Al_2O_3$), (MnOS), ($MnS.CaO.Al_2O_3.SiO_2$); and ($MnS.SiO_2$). During ESR most MnS, which have the most detrimental effects on toughness and ductility, are dissolved during the heating and melting of the consumable electrode at the slag-electrode interface during the formation of metal droplets from the liquid metal film. Subsequently, sulphur is removed according to equations (1) and (2a). The area fraction and total number of pure MnS are reduced in refining by 88 % and 78 % respectively and the maximum diameter is reduced from 15 to 5 µm.

$$[S]_{Metal} + \left(O^{2-}\right)_{Slag} \leftrightarrow \left(S^{2-}\right)_{Slag} + [O]_{Metal\ Drop} \quad (1)$$

$$3/2\ O_2(g) + \left(S^{2-}\right)_{Slag} \leftrightarrow \left(O^{2-}\right)_{Slag} + SO_{2\,(g)} \quad (2a)$$

During solidification, sulphides nucleate and grow on some oxide or nitride inclusions leading to multiphase inclusions with an oxide or nitride core surrounded by sulphide, e.g. ($MnS.Al_2O_3$), ($MnS.TiN.Al_2O_3$) as shown in Fig. 10 a and b. Other types of multiphase inclusions that are seen in small numbers, area fractions and maximum ECDs are ($MnS.CaO.Al_2O_3$), ($MnS.TiO_2$), (MnS. TiN), (MnS. (TiV)N), and (MnS.TiON). The precipitation of sulphide inclusions on oxides is commonly observed [29–31]. Kim et al. [16] concluded that increasing cooling rate reduces the incidence of MnS precipitation on oxides. In addition to pure MnS, a small amount of MnOS is re-precipitated during ESR, but with a lower number per mm^2, as well as a lower area fraction and diameter. Also, some sulphides are modified by Ca, e.g. forming (Ca.Mn) S and ($CaS.Al_2O_3$).

It is well known that the reaction between CaF_2 and Al_2O_3 according to equation (2b) leads to the formation of CaO which in turn, according to equation (3), can convert Al_2O_3 to $xCaO.yAl_2O_3$ inclusions that are softer and have a lower melting temperature than Al_2O_3 [22,32].

$$3CaF_2 + Al_2O_3 \rightarrow 3CaO + 2AlF_3(g) \quad (2b)$$

$$xCaO + yAl_2O_3 \rightarrow xCaO.yAl_2O_3 \quad (3)$$

The presence of traces of Ti in the steel and the small amount TiO_2 (0.13-0.15 wt.%) in the slag lead to the formation of $TiO_2.Al_2O_3.MnS$. Also, the high affinity of Ti and V for N lead to the formation of (TiV)N inclusions. The presence of TiO_2 at the high temperatures in the slag (1700-2000°C) [33] and the addition of Al metal allow the reduction of TiO_2 through an exothermic aluminothermic reduction reaction [34, 35] as in equation (4). Subsequently, once the Ti reaches the molten metal pool, TiN, (TiV)N, and TiO_2 are formed thereby explaining the presence of these types of inclusions in the ESR material while they are absent from the IF material.

$$4[Al] + 3(TiO_2) \rightleftharpoons 3[Ti] + 2(Al_2O_3) \quad (4)$$

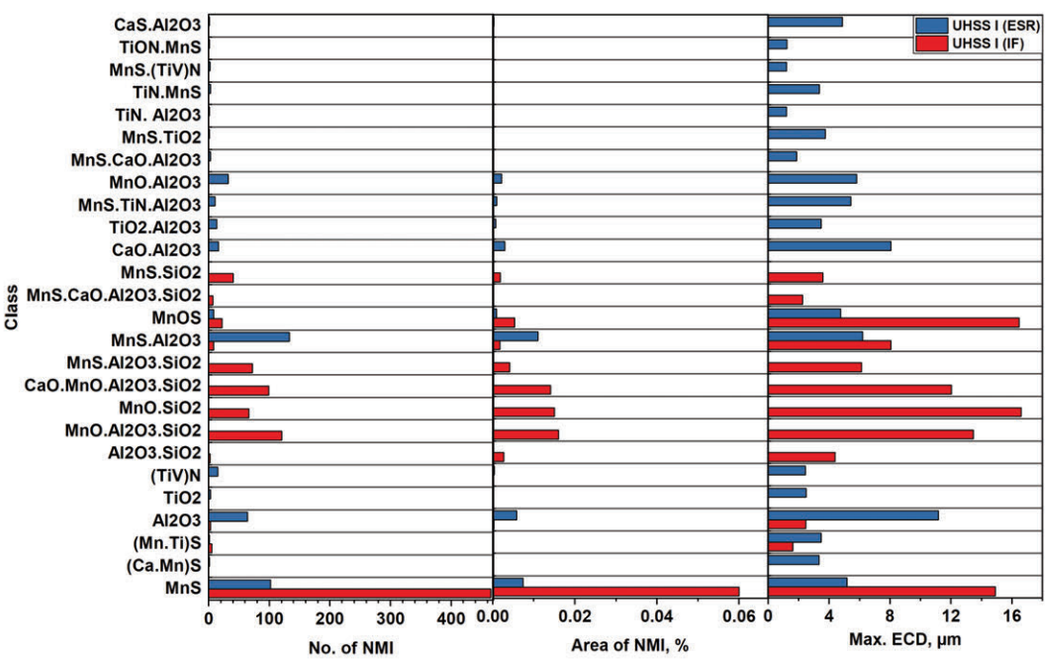

Figure 9. *Chemical compositions, numbers, area percentages, and maximum sizes of NMIs without and with ESR for UHSS I*

CC BY SA

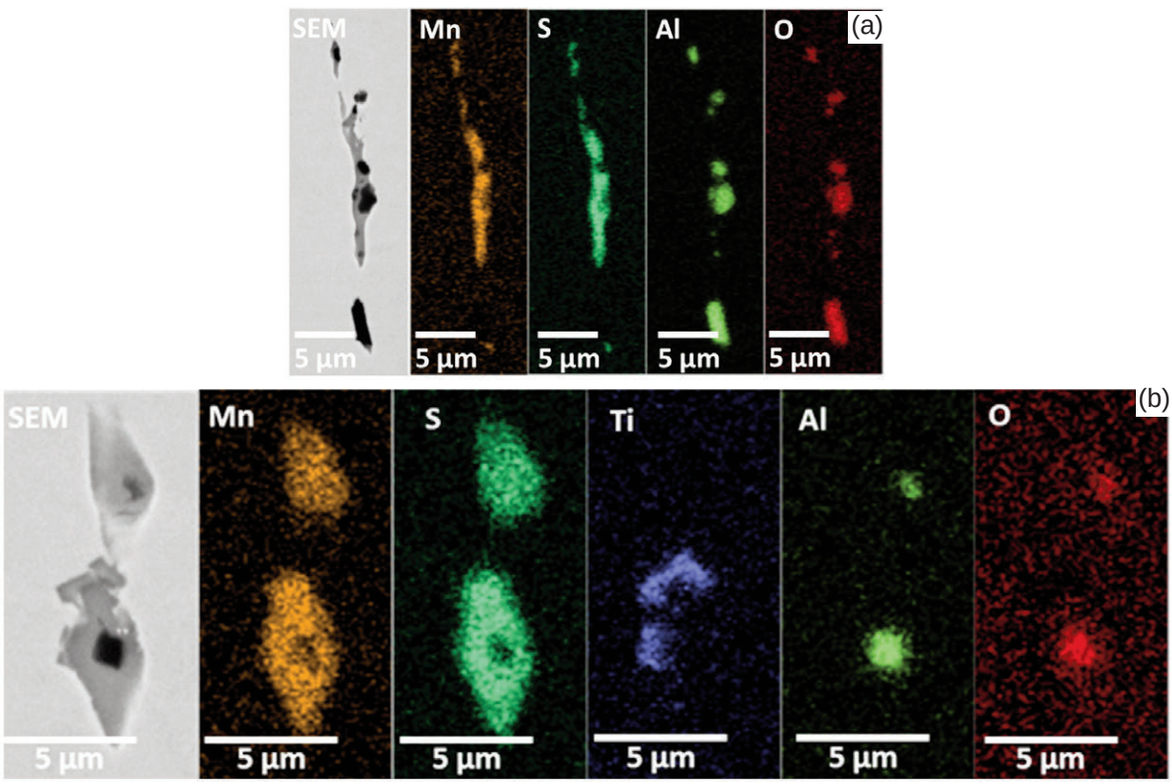

Figure 10. *EDS maps of deformed inclusions in UHSS I: (a) MnS.Al_2O_3 (b) MnS.TiN. Al_2O_3*

The spontaneity of the reaction presented in equation (4) was studied with thermodynamic calculations. The effect of aluminium and titanium activities at 1800 °C is illustrated in Fig. 11, in which the value of -305335 J/mol was used for the standard Gibbs free energy of the reaction, $\Delta G^0(4)$, as obtained from the software HSC Chemistry [26] version 9.6.1.

The thick black line in Fig. 11 illustrates the boundary in which the reaction presented in equation (4) is in equilibrium at 1800°C. It is calculated assuming that both titanium oxide and aluminium oxide are pure substances; i.e. their activities unity. This represents the case in which Al_2O_3 and TiO_2 exist in their own stoichiometric phases within the steel system; e.g. as inclusions. To the left of this line, reaction (4) is spontaneous from left to right, i.e. aluminium reacts with titanium oxide to produce titanium and aluminium oxide, and vice versa to the right of the line. Lowering the activity of titanium oxide (red lines in Fig. 11) transfers the boundary to the left. On the other hand, lowering the activity of aluminium oxide (blue lines in Fig. 11) transfers the boundary more to the right.

Fig. 11 also shows the activities of aluminium and titanium in the molten steel at 1800 °C for the six chemical compositions shown in Table 1. They were calculated with FactSage version 7.2 and its FsStel database. The open markers refer to compositions before ESR, whereas filled markers refer to compositions after the ESR. It can be seen that the activities of titanium and aluminium are in the area in which reaction (4) should occur spontaneously from left to right.

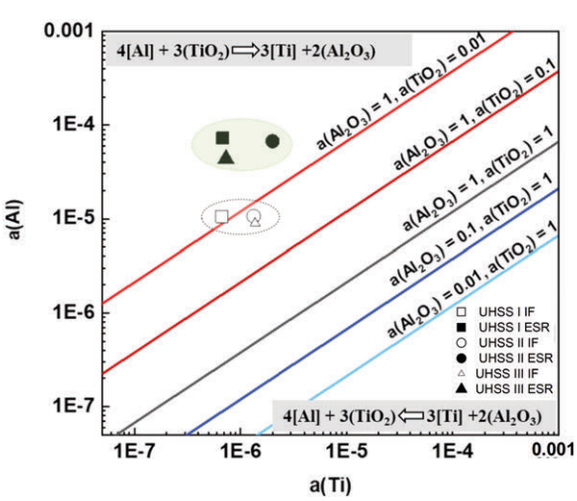

Figure 11. *Equilibrium of reaction (4) at 1800 °C as a function of the activities of aluminium and titanium and their oxides. In the top left-hand corner, reaction 4 goes left to right, while in the bottom right-hand corner it goes from right to left*

CC BY SA

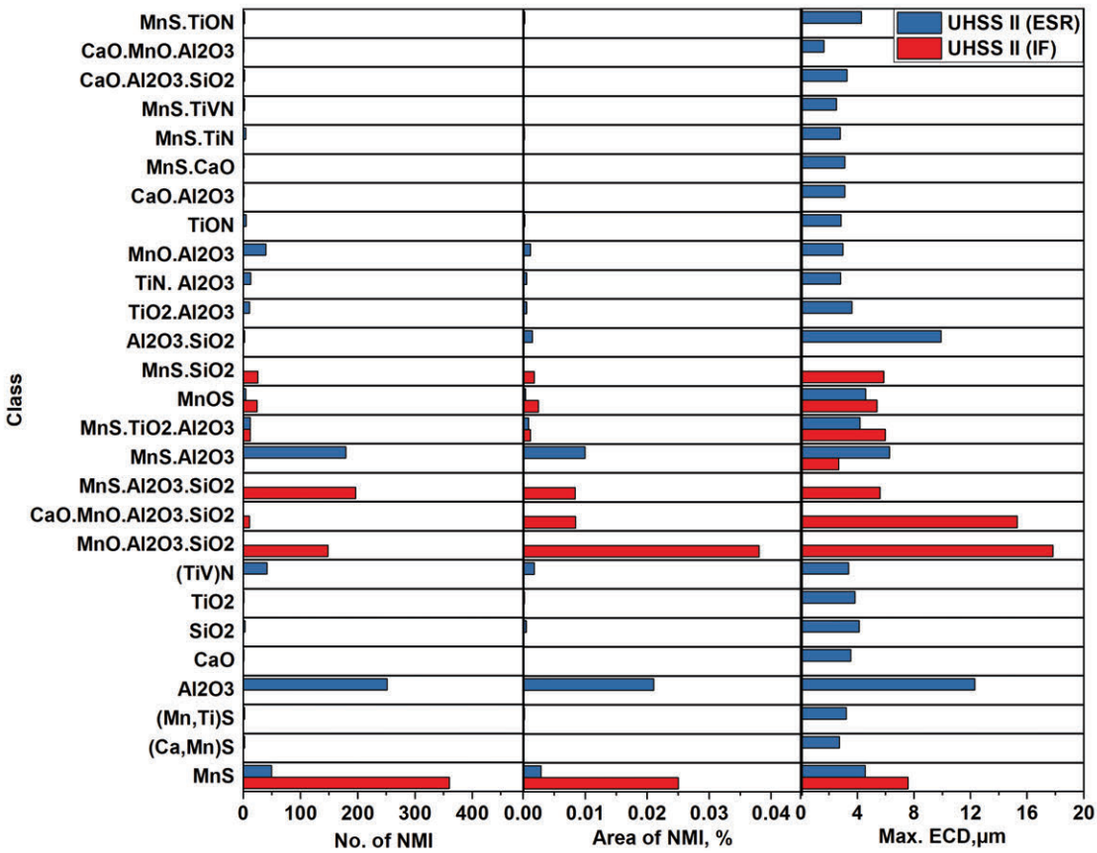

Figure 12. *Chemical compositions, numbers, area percentages, and maximum sizes of NMIs without and with ESR for UHSS II*

During the droplet formation at the tip of the electrode and due to the high temperature, hard and large oxide inclusions occupying large area fractions in UHSS I without ESR like ($Al_2O_3.SiO_2$),($MnO.Al_2O_3.SiO_2$),($MnO.SiO_2$), ($CaO.MnO.Al_2O_3.SiO_2$),($MnS.Al_2O_3.SiO_2$),and ($MnS.SiO_2$) were removed completely by dissolution [27, 36–38] after which the dissolved elements converted to other modified inclusions with a lower melting point, such as $xCaO.yAl_2O_3$, during cooling and solidification. This is in line with the observations of several other studies [39–44] that have shown that most oxide inclusions in the consumable electrode are removed before the metal droplets reach the molten metal pool. This dissolution mechanism was confirmed by the chemical compositions of the NMIs in the refined ingots, which were completely different from the NMIs in the consumable electrodes.

During the ESR process, at the slag-air interface, there is a continuous chemical reaction between the slag and oxygen in the air. Also, oxidation happens at the molten liquid film which forms on the tip of the electrode. To prevent atmospheric oxygen from entering the molten steel and to reduce the iron oxide formed, Al deoxidant was added to the ESR slag to

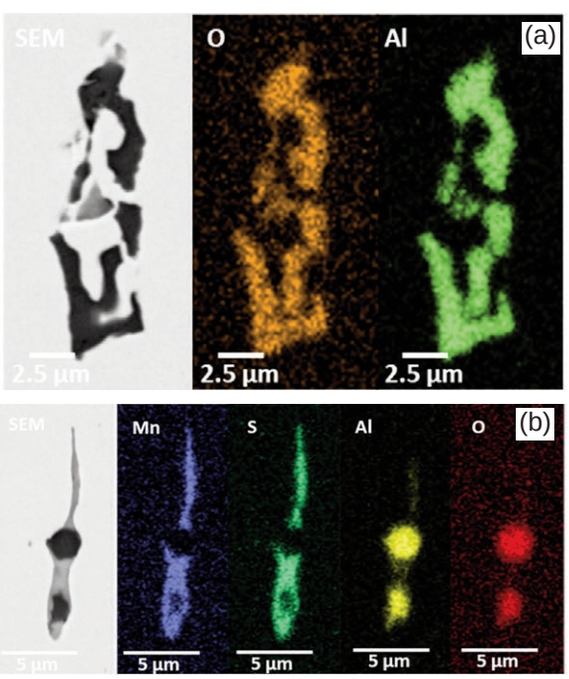

Figure 13. *EDS maps of deformed inclusions: (a) Al_2O_3 (b) $MnS.Al_2O_3$*

CC BY SA

bind oxygen according to the following reactions:

Reaction of added aluminium metal with atmospheric oxygen:

$$2[Al]_{in\ slag} + 3[O] \rightarrow (Al_2O_3) \quad (5)$$

Reduction of iron oxide in the liquid metal film:

$$2[Al]_{in\ slag} + 3(FeO) \rightarrow (Al_2O_3) + 3[Fe] \quad (6)$$

As can be seen from Fig. 15a, with ESR most alumina inclusions are less than 3 µm in size. Similar observations were made by Li et al [28]. The reason for this is that most of the Al_2O_3 generated in the liquid metal film is dissolved in the slag and the small amount of Al_2O_3 remaining within the droplet has no time to grow due to the short contact time between the slag and liquid metal film and due to high cooling rate in the ESR process which reduces NMI growth rates.

Table 1 shows that Al concentrations were increased as a result of ESR. This is undesirable, so further studies should be performed in order to reduce the total oxygen level without any increase in the Al concentration. Wang et al [45] concluded that the cleanliness of H13 ingots improved after adding aluminium during P-ESR due to a reduction in the number and size of NMIs. Typical $CaO.MnO.Al_2O_3.SiO_2$ inclusions in the consumable electrode were converted to Al_2O_3 particles in the P-ESR ingot. The results agreed with the results obtained by Zuzek et al. [46], who stated that ESR of 51CrV4 spring steel, produced by conventional continuous casting, led to a slight reduction in the concentration of impurities like S and P and other alloying elements, but it caused the appearance of some Al_2O_3 inclusions and an increase in the total Al concentration from 0.006 % to 0.025 %. Also, Shu et al [47] concluded that the NMIs in the consumable electrode of die steel, divided into large (MnCr)S and other large inclusions showing Al_2O_3 cores, were surrounded by (MnCr)S. All of these inclusions were removed by ESR except pure Al_2O_3 particles about 1 µm in size. These results were in agreement with those of Dong et al [22] who concluded that the main NMI observed in die steel is Al_2O_3 after ESR using conventional slag with the chemical composition 70% CaF_2, 30% Al_2O_3.

Some newly formed NMIs are removed during ESR by their floating up to the interface between the molten metal and the slag and then being absorbed

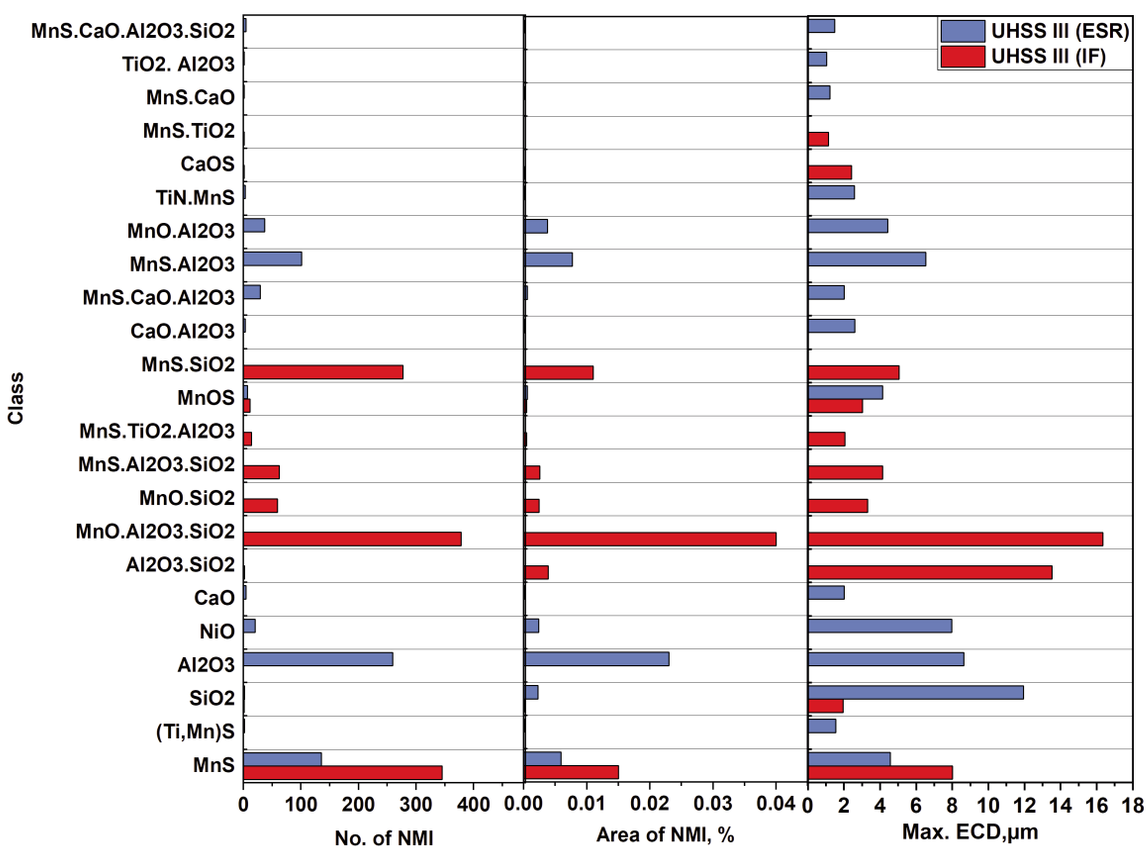

Figure 14. *Chemical compositions, numbers, area percentages, and maximum sizes of NMIs without and with ESR for UHSS III*

CC BY SA

by the slag, but this depends on the size of the NMI and the flotation velocity, which must be higher than the speed of the solidification front [39]. Despite their higher flotation velocities not all the large inclusions are removed in this way as illustrated in this study.

A sharp decrease in the area fraction, relative amount, and maximum diameter of MnS inclusions as a result of ESR was observed in UHSS II as shown in Fig. 12. However, part of the MnS inclusions are modified to (CaMn)S, (MnTi)S and part are reprecipitated on oxides or nitrides as ($MnS.Al_2O_3$), (MnS.CaO), (MnS.TiN), (MnS.TiVN), and (MnS.TiON). The inclusions ($MnO.Al_2O_3.SiO_2$), ($CaO.MnO.Al_2O_3.SiO_2$), ($MnS.Al_2O_3.SiO_2$), and ($MnS.SiO_2$) were removed completely by ESR. Fig. 15 b shows the size distribution of alumina (Al_2O_3) inclusions generated by ESR. They have a total area fraction of 0.021 %, and a maximum size of about 12 µm. Fig. 13 shows EDS mapping of the largest Al_2O_3 and ($MnS.Al_2O_3$) encountered. Other NMIs generated by ESR in small numbers and area fractions are (CaO,SiO_2), (TiO_2), (TiV)N, ($Al_2O_3.SiO_2$), ($TiO_2.Al_2O_3$), ($TiV.Al_2O_3$), ($MnO.Al_2O_3$), (TiON), and modified NMIs like ($CaO.Al_2O_3$), ($CaO.Al_2O_3.SiO_2$), and ($CaO.MnO.Al_2O_3$).

In UHSS III, complex NMIs such as ($Al_2O_3.SiO_2$), ($MnO.Al_2O_3.SiO_2$), ($MnO.SiO_2$), ($MnS.Al_2O_3.SiO_2$), ($MnS.TiO_2$. Al_2O_3), and ($MnS.SiO_2$) were removed completely and there was a sharp decrease in the area fraction, number and maximum diameter of MnS as a result of ESR. Fig. 15 c shows the size distribution of alumina inclusions generated by ESR. Their total area fraction is 0.023 % and maximum size about 8 µm. Other NMIs such as (MnTi) S, (NiO), (CaO), ($CaO.Al_2O_3$), (MnS. $CaO.Al_2O_3$), ($MnS.Al_2O_3$), ($MnO.Al_2O_3$), (TiN.MnS), (CaOS), ($MnS.TiO_2$), (MnS.CaO),($TiO_2.Al_2O_3$), and ($MnS.CaO.Al_2O_3.SiO_2$) were generated by ESR in small numbers and very low area fractions as shown in Fig. 14.

From Fig. 15, it can be seen that 98% of the total detected pure Al_2O_3 inclusions are smaller than 6 µm for UHSS I while the corresponding percentages for UHSS III and UHSS II are 97% and 95%, respectively. Measured this way, the best degree of refining is obtained with UHSS I and III followed by UHSS II.

3.3 Thermodynamic Calculations

With the software available, it was not possible to calculate slag - steel equilibrium because the software was not applicable to slags with high CaF_2 contents. However, using FactSage 7.2 [25] with various databases (FSstel, FToxid, and FactPS) it was possible to calculate the expected NMI compositions based on the chemical compositions of the steels in Table 1, as shown in Fig. 16.

Fig. 16 shows that in all cases, in agreement with the results presented above, the predicted amount and types of NMIs should decrease as a result of ESR due to the slight change in the chemical composition of the steel and the reduction in the level of impurities. However, the chemical compositions of some of the predicted types of NMIs after ESR are slightly different from the observed NMIs. For example, AlN and Ti(CS), which were predicted in the thermodynamic calculations, are not found experimentally. This is because of the effect of the slag that is omitted from the calculations. During the ESR process, due to the high affinity of Al to oxygen, the oxygen in the slag consumes most of the Al added to form Al_2O_3 in the liquid steel. Therefore, more N is available for the formation of TiN. During solidification, MnS nucleate and grow on some oxide or nitride inclusions such as Al_2O_3 and TiN leading to the multiphase inclusions $MnS.Al_2O_3$ and TiN.MnS. The figure shows that the mass fraction of MnS, which represents the main NMIs in the IF material, is reduced as a result of ESR. Titanium oxide and all the predicted complex NMIs such as manganese aluminate, manganese aluminium silicate, and molten inclusions are predicted to be removed completely as a result of ESR. Molten inclusions refer to inclusions in the molten state at the calculation temperatures. They are rich in Mn, Al and Si and O with other impurities e.g. S and light

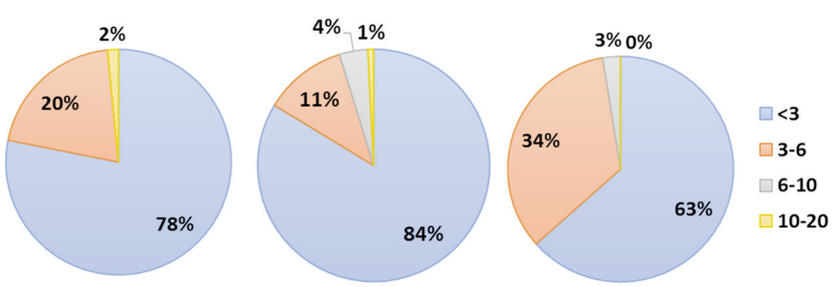

Figure 15. *Size distribution of Al_2O_3 formed as a result of ESR in UHSS I (a), UHSS II (b) and UHSS III (c)*

CC BY SA

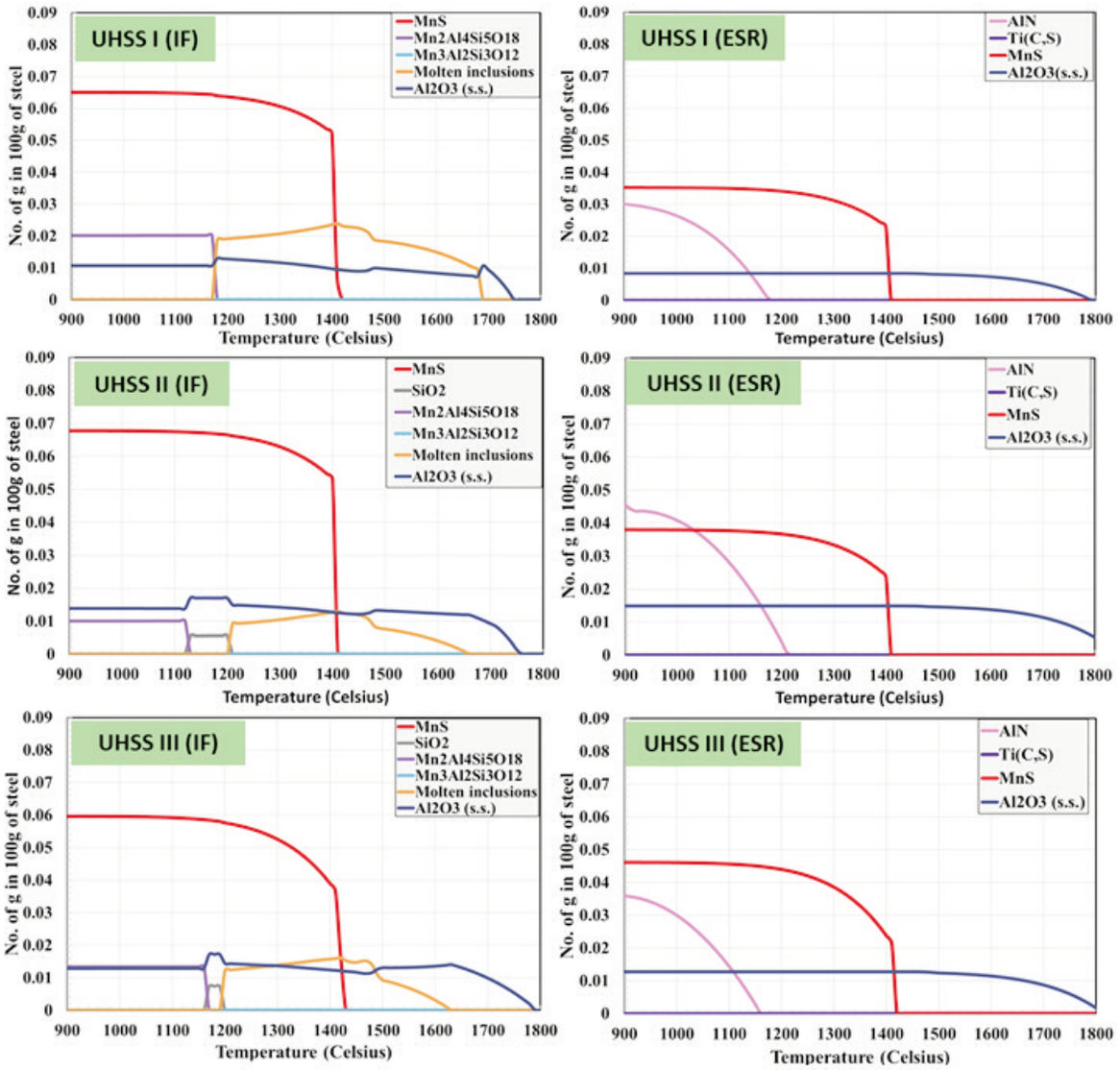

Figure 16. *Thermodynamic calculations of the expected NMIs in the investigated steels without and with ESR*

elements e.g. Ti. Their compositions varied significantly with temperature, so it is preferable to call them molten inclusions without exact stochiometric chemical compositions.

4. Conclusion

With the aim of obtaining good combinations of strength and toughness, three ultrahigh-strength steels containing different amounts of C, Cr, Ni, Mn, and Si were melted in an induction furnace and then refined using ESR technology with a slag based on CaF_2. A detailed investigation of the original and secondary non-metallic inclusions in bars forged from the induction melted ingots and the ESR ingots were made. The following conclusions can be drawn.

1. ESR using a slag comprising of 70% CaF_2, 15% Al_2O_3, and 15% CaO enhances the cleanliness of UHSSs by decreasing the total impurity level (O%+N%+S%) and non-metallic inclusion content by as much as 46 % and 62 % respectively.

2. In all the ESR treated steels, NMIs smaller than 6 µm represent about 94 % of the total inclusion counts as compared with 90 % without ESR.

3. ESR results in the formation of new NMIs like $MnS.Al_2O_3$ and TiN.MnS which were formed as a result of MnS reprecipitation on oxide or nitride inclusions. These NMIs were relatively scarce in number density and showed small area percentages and maximum ECDs. Some sulphides are modified by Ca to (CaMn)S and $CaS.Al_2O_3$. Some nitrides like TiN and (TiV)N are nucleated and precipitated during

CC BY SA

the solidification phase.

4. Small Al_2O_3 particles were formed in the steels as a result of an addition of Al to the slag at the beginning of the ESR process for deoxidation and protection of the molten metal pool from attack by atmospheric oxygen. Up to 98 % of the particles have equivalent circle diameters less than 6μm. Also, adding Al to the slag led to an increase in the total Al content of the ESR ingots.

5. Thermodynamic calculations show good agreement with the experimental results. The predicted mass fraction of MnS inclusions, which represent the main NMIs, decreases as a result of ESR. Silicon oxides and all predicted complex NMIs such as manganese aluminium silicate and molten inclusions are predicted to be completely removed as a result of ESR.

6. The effect of ESR on the cleanliness of the investigated steels not only depends on the process parameters, but also on the chemical compositions and total impurity levels in the consumable electrode.

Acknowledgment

The authors acknowledge the Egyptian Ministry of Higher Education (Cultural Affairs and Missions Sector) for the financial support during this work.

References

[1] D. Morris, D. James, Eglin steel-a low alloy high strength composition, US 7,537,727 B2, 2009.

[2] L.U. Yan, S.U. Jie, W. Junhua, X.I.E. Gang, Y. Zhuoyue, Acta Metall. Sin. Engl. Lett., 24 (2011) 423–431.

[3] G. Vartanov, High strength military steel, US 8,414.713 B2, 2013.

[4] Y. Ren, Y. Wang, S. Li, L. Zhang, X. Zuo, S.N. Lekakh, K. Peaslee, Metall. Mater. Trans. B. ,45 (2014) 1291–1303.

[5] Z.G. Yang, S.X. Li, J.M. Zhang, J.F. Zhang, G.Y. Li, Z.B. Li, W.J. Hui, Y.Q. Weng, Acta Mater., 52 (2004) 5235–5241.

[6] M.D. Chapetti, T. Tagawa, T. Miyata, Mater. Sci. Eng. A., 356 (2003) 227–235.

[7] M.D. Chapetti, T. Tagawa, T. Miyata, Mater. Sci. Eng. A,. 356 (2003) 236–244.

[8] L.H. He, J.H. Zhao, Int. J. Eng. Sci., 38 (2000) 1181–1195.

[9] C. Bertrand, J. Molinero, S. Landa, R. Elvira, M. Wild, G. Barthold, P. Valentin, H. Schifferl, Ironmak. Steelmak., 30 (2003) 165–169.

[10] E.A. Chichkarev, Metallurgist., 54 (2010) 236–243.

[11] D. Janke, Z. Ma, P. Valentin, A. Heinen, ISIJ Int., 40 (2000) 31–39.

[12] S. Yang, Q. Wang, L. Zhang, J. Li, K. Peaslee, Metall. Mater. Trans. B., 43 (2012) 731–750.

[13] P. Kaushik, J. Lehmann, M. Nadif, Metall. Mater. Trans. B., 43 (2012) 710–725.

[14] L. Zhang, B.G. Thomas, ISIJ Int., 43 (2003) 271–291.

[15] B.-H. Yoon, K.-H. Heo, J.-S. Kim, H.-S. Sohn, Ironmak. Steelmak., 29 (2002) 214–217.

[16] H.S. Kim, H.-G. Lee, K.-S. Oh, Met. Mater., 6 (2000) 305–310.

[17] A.K. Vaish, G.V.R. Iyer, P.K. De, B.A. Lakra, A.K. Chakrabarti, P. Ramachandrarao, J. Metall. Mater. Sci. 42 (2000) 11–29.

[18] W.E. Duckworth, G. Hoyle, Electro-slag refining, Chapman & Hall, 1969.

[19] U. Biebricher, H. Scholz, Metall. Plant Technol. Int. 22 (1998) 36–38.

[20] T. Mattar, J. Mater. Sci. Technol. MST. 17 (2009) 35–46.

[21] T. Mattar, in: 6th Int. Tool. Conf. Karlstad, 2002, p. 10–13.

[22] Y.-W. Dong, Z.-H. Jiang, Y.-L. Cao, A. Yu, D. Hou, Metall. Mater. Trans. B., 45 (2014) 1315–1324.

[23] M. Ali, M. Eissa, H.E. Faramawy, D. Porter, J. Kömi, M.F. El-Shahat, T. Mattar, J. Miner. Mater. Charact. Eng., 05 (2017) 385–407.

[24] M. Li, D. Wilkinson, K. Patchigolla, Part. Sci. Technol., 23 (2005) 265–284.

[25] C.W. Bale, E. Bélisle, P. Chartrand, S.A. Decterov, G. Eriksson, A.E. Gheribi, K. Hack, I.-H. Jung, Y.-B. Kang, J. Melançon, A.D. Pelton, S. Petersen, C. Robelin, J. Sangster, P. Spencer, M.-A. Van Ende, Calphad., 54 (2016) 35–53.

[26] HSC Chemistry, (n.d.). http://www.hsc-chemistry.com/.

[27] J. Burja, F. Tehovnik, M. Godec, J. Medved, B. Podgornik, R. Barbic, J. Min. Metall. Sect. B Metall. 54 (2018) 51–57.

[28] S. Li, G. Cheng, Z. Miao, W. Dai, L. Chen, Z. Liu, ISIJ Int. (2018) 1-10.

[29] H. Doostmohammadi, P.G. Jönsson, J. Komenda, S. Hagman, Steel Res. Int., 81 (2010) 142–149.

[30] K. Oikawa, K. Ishida, T. Nishizawa, ISIJ Int., 37 (1997) 332–338.

[31] M. Wakoh, T. Sawai, S. Mizoguchi, ISIJ Int. ,36 (1996) 1014–1021.

[32] R.H. Nafziger, The Electroslag Melting Process, U.S. Bureau of Mines, 1974.

[33] U.B. Pal, C.J. MacDonald, E. Chiang, W.C. Chernicoff, K.C. Chou, J. Van Den Avyle, M.A. Molecke, D. Melgaard, Metall. Mater. Trans. B., 32 (2001) 1119–1128.

[34] M. Maeda, T. Yahata, K. Mitugi, T. Ikeda, Mater. Trans. JIM., 34 (1993) 599–603.

[35] S. Duan, X. Shi, M. Mao, W. Yang, S. Han, H. Guo, J. Guo, Sci. Rep., 8 (2018) 1-14.

[36] B. Arh, B. Podgornik, J. Burja, Mater. Tehnol., 50 (2016) 971–979.

[37] L. Yang, G. Cheng, S. Li, M. Zhao, G. Feng, ISIJ Int., 55 (2015) 1901–1905.

[38] L. Yang, G. Cheng, Int. J. Miner. Metall. Mater., 24 (2017) 869–875.

[39] D.A.R. Kay, R.J. Pomfret, J Iron Steel Inst., 209 (1971) 962–965.

[40] J. Fu, J. Zhu, Acta Met. Sin., 7 (1964) 250–262.

[41] D. Zhou, X. Chen, J. Fu, P. Wang, J. Li, M. Xu, J. Univ.

Sci. Technol. Beijing China., 22 (2000) 26–30.
[42] Z.B. Li, W.H. Zhou, Y.D. Li, Iron Steel., 15 (1980) 20–26.
[43] Z.B. Li, J.W. Zhang, X.Q. Che, J Iron Steel Res., 9 (1997) 7.
[44] A. Mitchell, Ironmak. Steelmak., 1 (1974) 172–179.
[45] F. Wang, X.C. Chen, H.J. Guo, in: Adv. Mater. Res., Trans Tech Publ., 2012: pp. 218–226.
[46] B. Zuzek, M. Sedla, B. Podgornik, Frat. Ed Integrità Strutt., 34(2015) 160-168.
[47] C.-B. Shi, X.-C. Chen, H.-J. Guo, Z.-J. Zhu, H. Ren, Steel Res. Int., 83 (2012) 472–486.

UTICAJ ELEKTRIČNOG PRETAPANJA POD TROSKOM NA ČISTOĆU CrNiMoWMnV ČELIKA ULTRAVISOKE ČVRSTOĆE

M. Ali [*a,c], D. Porter [a], J. Kömi [a], E.-P. Heikkinen [b], M. Eissa [c], H. El Faramawy [c], T. Mattar [c]

[a*] Univerzitet u Oulu, Fakultet za materijale i mašinstvo, Centar za napredna istraživanja čelika, Oulu, Finska
[b] Univerzitet u Oulu, Laboratorija za procesnu metalurgiju, Oulu, Finska
[c] Odsek za obradu čelika, Centralni institut za metalurška istraživanja i razvoj (CMRDI), Helvan, Kairo, Egipat

Apstrakt

U ovom radu je ispitivana čistoća čelika ultravisoke čvrstoće (UHSSs) bez i nakon obrade rafinacionim postupkom električnog pretapanja pod troskom (ESR) sastava 70% CaF_2, 15% Al_2O_3 i 15% CaO. Tri uzorka čelika ultravisoke čvrstoće različitog hemijskog sastava su pripremljeni u indukcionoj peći i rafinisani ESR postupkom. Izliveni ingoti su kovani na temperaturi između 950 i 1100°C, zatim su hlađeni na vazduhu, a karakterizacija njihovih nemetaličnih uključaka je urađena skenirajućim elektronskim mikrosopom sa emisijom polja i laserskim skenirajućim konfokalnim mikroskopom. Za termodinamičke proračune očekivanih nemetaličnih uključaka u ispitivanim čelicima sa i bez ESR postupka rafinacije korišćen je FactSage 7.2 softver, dok je Chemistry version 9.6.1softver korišćen za izračunavanje standardne Gibsove slobodne energije (ΔG°). Rezultati su pokazali da se kod čelika nakon ESR postupka ukupni nivo nečistoća (TIL% = O% + N% + S%), kao i sadržaj nemetaličnih uključaka, smanjio za 46%, odnosno 62%. Nemetalični uključci su klasifikovani u četiri glavne klase: oksidi, sulfidi, nitridi i kompleksni multifazni uključci. Postupak ESR rafinacije je doveo do velikih promena u procentima, gustini, maksimalnih prečnika ekvivalentnih krugova, kao i hemijskog sastava različitih nemetaličnih uključaka. Većina MnS nemetaličnih uključaka je bila uklonjena, mada su se neki ponovo nataložili na oksidne i nitridne uključke što je dovelo do stvaranja multifaznih uključaka sa oksidnim ili nitridnim jezgrom okruženih sulfidima, kao što su ($MnS.Al_2O_3$) i (MnS. TiN). Neki sulfidi su se takođe modifikovali u prisustvu Ca i formirali (CaMn)S i $CaS.Al_2O_3$. Neki nitridi, kao što su TiN i (TiV)N, su obrazovali jezgro i nataložili se tokom faze solidifikacije. Uključci Al_2O_3 su nastali kao rezultat dodavanja Al kao deoksidanta ESR trosci da bi se sprečilo prodiranje kiseonika u rastopljeni čelik.

Ključne reči: *Čelik ultravisoke čvrstoće; Električno pretapanje šljake; Sintetička šljaka; Nemetalični uključci; Čistoća*